Ab Initio Calculations on 1,3,5-Trimethylenebenzene and Its Negative Ion Provide Predictions about the Photoelectron Spectrum of the Ion

Carl R. Kemnitz,[†] Robert R. Squires,[‡] and Weston Thatcher Borden*[,†]

Contribution from the Department of Chemistry, Box 351700, University of Washington, Seattle, Washington 98195-1700, and Department of Chemistry, Purdue University, West Lafayette, Indiana 47907

Received January 21, 1997[⊗]

Abstract: The results of *ab initio* calculations on 1,3,5-trimethylenebenzene (**1**) and its negative ion (**1**$^-$) are presented. Geometries were optimized at the CASSCF/6-31G* and CASSCF/6-31+G* levels. Single-point calculations were performed using second-order perturbation and multireference configuration interaction (MR-CI) methods, in order to include the effects of dynamic correlation between the σ and π electrons. The ground state of **1** is predicted to be the high spin $^4A_1''$ state, which has D_{3h} symmetry. The lowest energy excited state is $^2E''$ in D_{3h} symmetry and is thus subject to first-order Jahn−Teller distortions to geometries of lower symmetry. The C_{2v} geometries of the two Jahn−Teller distorted components of $^2E''$, $^2B_1$ and $^2A_2$, have been optimized and are found to have nearly the same energies. After correction for zero-point energy differences, the adiabatic energy separation between the lowest C_{2v} doublet and the D_{3h} quartet ground state of **1** is computed to be 14 ± 1 kcal/mol. The ground state of **1**$^-$ is predicted to be $^3E'$ in D_{3h} symmetry. Molecular distortion to C_{2v} symmetry stabilizes the $^3B_2$ component of $^3E'$ via not only first- but also second-order Jahn−Teller effects. Consequently, the $^3B_2$ component of $^3E'$, at its optimized geometry, is calculated to be lower in energy by ca. 1.5 kcal/mol than the $^3A_1$ component at its optimized geometry. The lowest singlet excited state of **1**$^-$ is $^1A_1'$ in D_{3h} symmetry, which is predicted to undergo second-order Jahn−Teller distortions, at least at the CASSCF level of theory. The resulting state, $^1A_1$ in C_{2v} symmetry, is calculated to be 4−6 kcal/mol above the $^3B_2$ ground state but slightly below a $^3A_2'$ excited state of D_{3h} symmetry. In contrast to CASSCF and MR-CI, UB3LYP/6-31+G* calculations predict $^3A_2'$ to be the ground state of **1**$^-$, slightly below either component of the Jahn−Teller distorted $^3E'$ state. The UB3LYP calculations afford an estimate of 21−22 kcal/mol for the electron affinity of **1** and provide vibrational frequencies for the $^4A_1''$ state. On the basis of computational results for **1** and **1**$^-$, the most important features of the photoelectron spectrum of **1**$^-$ are predicted.

The qualitative understanding of the properties of molecules that potentially have a large number of unpaired electrons in the ground state[1] has evolved from theoretical[2] and experimental[1,3] studies of diradicals. Extending these detailed studies to triradicals is an obvious next step, and 1,3,5-trimethylenebenzene (**1**) is a triradical of particular interest. Trimethylenebenzene is a non-Kekulé alternant hydrocarbon in which three electrons occupy three nonbonding molecular orbitals (NBMOs); thus, **1** has both doublet and quartet spin states.

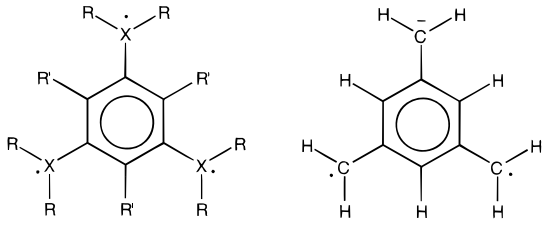

1, R = R' = H, X = C
2, R = C_6Cl_5, R' = Cl, X = C
3, R = R' = H, X = N^+

1$^-$

A sterically hindered, perchlorinated trimethylenebenzene derivative (**2**) has been recently characterized as a ground state quartet that is stable indefinitely under ambient conditions and can even withstand heating to 250 °C in air.[4] In contrast, a sterically congested tris(*tert*-butyl nitroxide) analog of **1** has been found to have a doublet ground state.[5] Replacing the peripheral methylene groups in **1** with amino radical cations, as in **3**, may allow redox switching of the magnetic properties.[6] Incorporation of triradical building blocks, based on **1**, into larger molecular assemblies provides a possible strategy for achieving bulk ferromagnetism.[1]

A complete understanding of the electronic structure of **1** requires a reliable knowledge of the relative energies of the low-lying electronic states. Negative ion photoelectron spectroscopy[7] provides a means to obtain accurate state splittings in

[†] University of Washington.
[‡] Purdue University.
[⊗] Abstract published in *Advance ACS Abstracts,* June 15, 1997.

(1) For reviews on high-spin organic molecules, see: (a) Dougherty, D. E. *Acc. Chem. Res.* **1991**, *24*, 88. (b) Iwamura, H.; Koga, N. *Acc. Chem. Res.* **1993**, *26*, 346. (c) Iwamura, H. *Adv. Phys. Org. Chem.* **1990**, *26*, 179. (d) Rajca, A. *Chem. Rev.* **1994**, *94*, 871.

(2) For reviews, see: (a) Borden, W. T. In *Diradicals*; Borden, W. T., Ed.; Academic Press: New York, 1982; Chapter 1. (b) Borden, W. T. *Mol. Cryst. Liq. Cryst.* **1993**, *232*, 195.

(3) For reviews, see: (a) Berson, J. A. In *Diradicals*; Borden, W. T., Ed.; Academic Press: New York, 1982; Chapter 3. (b) Platz, M. S. In *Diradicals*; Borden, W. T., Ed.; Academic Press: New York, 1982; Chapter 5. (c) *Kinetics and Spectroscopy of Carbenes and Biradicals*; Platz, M. S., Ed; Plenum Press, New York, 1990. (d) Borden, W. T.; Iwamura, H.; Berson, J. A. *Acc. Chem. Res.* **1994**, *27*, 109.

(4) Veciana, J; Rovira, C.; Ventosa, N.; Crespo, M. I.; Palacio, F. *J. Am. Chem. Soc.* **1993**, *115*, 57.

(5) Fujita, J.; Tanaka, M.; Suemune, H.; Koga, N.; Matsuda, K.; Iwamura, H. *J. Am. Chem. Soc.* **1996**, *118*, 9347.

(6) (a) Stickley, K. R.; Blackstock, S. C. *J. Am. Chem. Soc.* **1994**, *116*, 11576. (b) Wienk, M. M.; Janssen, R. A. J. *J. Am. Chem. Soc.* **1997**, *119*, 4492.

(7) For a review of negative ion photoelectron spectroscopy, see: Ervin, K. M.; Lineberger, W. C. In *Advances in Gas Phase Ion Chemistry*; Adams, N., Babcock, L. M., Eds.; JAI Press: London, England, 1992; Vol. 1, pp 121−166.

S0002-7863(97)00195-9 CCC: $14.00

open-shell molecules such as **1**, provided the corresponding gaseous negative ion is available. Hu and Squires have recently reported the generation of trimethylenebenzene negative ion, $\mathbf{1}^-$, in the gas phase.[8] The observed reactivity of this "distonic diradical anion" was suggestive of a triplet ground state. Triplet carbanions are quite unusual, and therefore, a theoretical understanding of the electronic structure of $\mathbf{1}^-$ is also of considerable interest.

Herein, we present the results of *ab initio* calculations on **1** and $\mathbf{1}^-$ that have been carried out with multiconfigurational methods and the inclusion of dynamic electron correlation, both of which are necessary to calculate reliably the energy separations between the different spin states of a triradical such as **1**[9,10] and of a diradical such as $\mathbf{1}^-$. A primary impetus for this work was to predict the major features of the photoelectron spectrum of diradical $\mathbf{1}^-$, prior to its measurement. The photoelectron spectra of the radical anions of trimethylenemethane,[11] *m*-benzoquinodimethane,[12] and cyclooctatetraene,[13] which have been obtained very recently, have shown that prior *ab initio* calculations on the neutral diradicals[14−16] gave remarkably good predictions of the singlet−triplet energy differences that were measured. Indeed, the calculated geometries and vibrational frequencies of both the radical anions and the neutral diradicals were essential aids for the final spectral assignments that were reported. Similarly, the computational results reported here should facilitate the analysis of the photoelectron spectrum of $\mathbf{1}^-$.

Theoretical Considerations

The electronic structures of **1** and $\mathbf{1}^-$ can be qualitatively understood in terms of their NBMOs. Longuet-Higgins showed that in a neutral non-Kekulé alternant hydrocarbon such as **1** the number of atoms which cannot be included in π bonds is equal to both the number of π NBMOs and the number of electrons that occupy them.[17] Thus, in **1**, a total of three electrons occupy three NBMOs. The Hückel NBMOs are easily obtained from the zero-sum rule,[17] and they are schematically depicted in Figure 1. In D_{3h} symmetry one NBMO is a_2''; together, the remaining pair belong to the degenerate e″ representation.

The three NBMOs of **1** have atoms in common (i.e., they are nondisjoint). Therefore, the Coulombic repulsion between the three electrons that occupy the NBMOs will be minimized when the electrons each occupy a different MO and all have parallel spins.[2,18] The same prediction of a quartet ($S = {}^3/_2$) ground state can be made using valence-bond theory.[19]

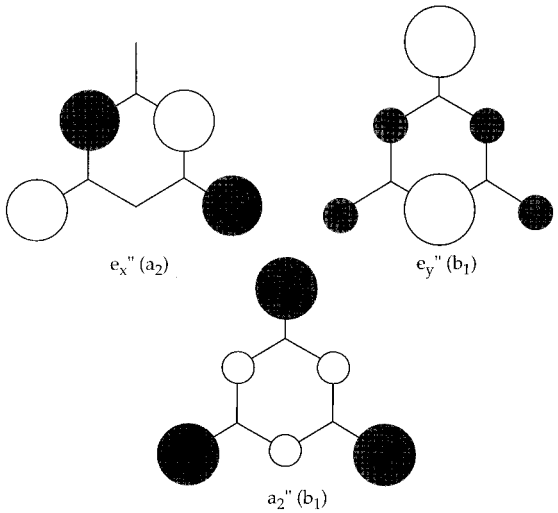

Figure 1. Schematic depiction of the π NBMOs of **1**. The orbital energy of a_2'' is 1.5 kcal/mol lower than that of e″ in an ROHF/6-31G* calculation on $^4A_1''$.

The configurations with $S_z = {}^1/_2$ that can be formed by placing three electrons in the three NBMOs are shown in Figure 2. A spin eigenvalue of ${}^1/_2$ along one axis is possible not only for the doublet states ($S = {}^1/_2$ and $S_z = \pm{}^1/_2$) but also the quartet state ($S = {}^3/_2$ and $S_z = \pm{}^3/_2$ and $\pm{}^1/_2$). The $S_z = \pm{}^3/_2$ components of the quartet (not shown in Figure 2) have one electron in each NBMO with the same spin along the *z* axis.

When one or all three electrons occupy the degenerate pair of e″ NBMOs, each configuration belongs to one component, either $^2E_x''$ or $^2E_y''$, of a degenerate $^2E''$ pair. However, when two electrons occupy the e″ NBMOs, individual configurations do not belong to an irreducible representation of D_{3h}; only linear combinations of configurations can be assigned a symmetry designation. In fact, as shown in Figure 2, three different linear combinations of configurations g, h, and i give rise to 2 $^2E_x''$, $^2A_1''$, and the $S_z = {}^1/_2$ component of the $^4A_1''$ state. Clearly, multiconfigurational methods must be used to provide even a minimally correct description of the low-lying states of **1**.

The $^2E''$ states should be subject to first order Jahn−Teller distortions which lift their D_{3h} degeneracy.[20] The pair of e′ molecular distortions depicted in Figure 3 deform the carbon skeleton of **1** in the required manner. A salient feature of the phase of the e_y' mode shown in Figure 3 is that it lengthens the exocyclic C−C bond that lies along the C_2 axis labeled 1 and shortens the other two exocyclic C−C bonds. We will, therefore, call this phase of the e_y' distortion mode the "long-short-short" (l-s-s) distortion. The opposite phase (s-l-l) of the same e_y' mode produces a different C_{2v} structure with a short exocyclic bond along the same C_2 axis and long bonds to the other two exocyclic carbons.

Since there are three C_2 axes in **1** at a D_{3h} geometry, there are three equivalent l-s-s and three equivalent s-l-l distortions of **1** to structures with C_{2v} symmetry (Figure 4). Pseudorotation between each pair of the three equivalent l-s-s structures involves passage through one of the equivalent s-l-l structures at the midway point and *vice versa*. The three equivalent C_{2v} structures of one type are expected to be minima along the

(8) Hu, J.; Squires, R. R. *J. Am. Chem. Soc.* **1996**, *118*, 5816.
(9) Previous *ab initio* calculations[10] on **1** have been performed without the use of multiconfigurational wave functions and/or without provision for dynamic electron correlation.
(10) (a) Yoshizawa, K.; Hatanaka, M.; Ito, A.; Tanaka, K.; Yamabe, T. *Chem. Phys. Lett.* **1993**, *202*, 483. (b) Yoshizawa, K.; Hatanaka, M.; Ito, A.; Tanaka, K.; Yamabe, T. *Mol. Cryst. Liq. Cryst.* **1993**, *232*, 323. (c) Yoshizawa, K.; Hatanaka, M.; Matsuzaki, Y.; Tanaka, K.; Yamabe, T. *J. Chem. Phys.* **1994**, *100*, 4453. (d) Raos, G.; Gerratt, J.; Cooper, D. L.; Raimondi, M. *Chem. Phys.* **1994**, *186*, 251. (e) Li, S.; Ma, J.; Jiang, Y. *J. Phys. Chem.* **1996**, *100*, 4775. (f) Zhang, J.; Baumgarten, M. *Chem. Phys. Lett.* **1997**, *269*, 187.
(11) Wenthold, P. G.; Hu, J.; Squires, R. R.; Lineberger, W. C. *J. Am. Chem. Soc.* **1996**, *118*, 475.
(12) Wenthold, P. G.; Kim, J. B.; Lineberger, W. C. *J. Am. Chem. Soc.* **1997**, *119*, 1354.
(13) Wenthold, P. G.; Hrovat, D. A.; Borden, W. T.; Lineberger, W. C. *Science* **1996**, *272*, 1456.
(14) A complete list of calculations on trimethylenemethane is given in ref 11.
(15) (a) Kato, S.; Morokuma, K.; Feller, D.; Davidson, E. R.; Borden, W. T. *J. Am. Chem. Soc.* **1983**, *105*, 1791. (b) Fort, R. C., Jr.; Getty, S. J.; Hrovat, D. A.; Lahti, P. M.; Borden, W. T. *J. Am. Chem. Soc.* **1992**, *114*, 2549.
(16) Hrovat, D. A.; Borden, W. T. *THEOCHEM.* In press.
(17) Longuet-Higgins, H. C. *J. Chem. Phys.* **1950**, *18*, 265.
(18) Borden, W. T.; Davidson, E. R. *J. Am. Chem. Soc.* **1977**, *99*, 4587.
(19) Ovchinnikov, A. A. *Theor. Chim. Acta* **1978**, *47*, 297.
(20) Jahn, H. A.; Teller, E. *Proc. R. Soc. London, Ser. A* **1937**, *161*, 220.

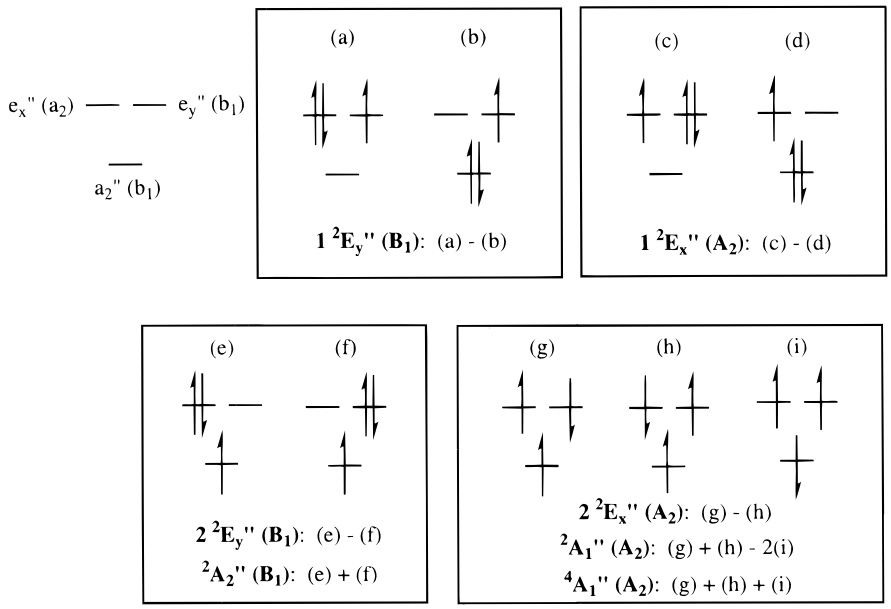

Figure 2. The $S_z = {}^1/_2$ configurations for D_{3h} states of **1**. C_{2v} symmetries are given in parentheses. The $S_z = {}^3/_2$ component of $^4A_1''$, like the $S_z = {}^1/_2$ component, shown here, has one electron in each NBMO; but in the $S_z = {}^3/_2$ component, all three electrons have α spin.

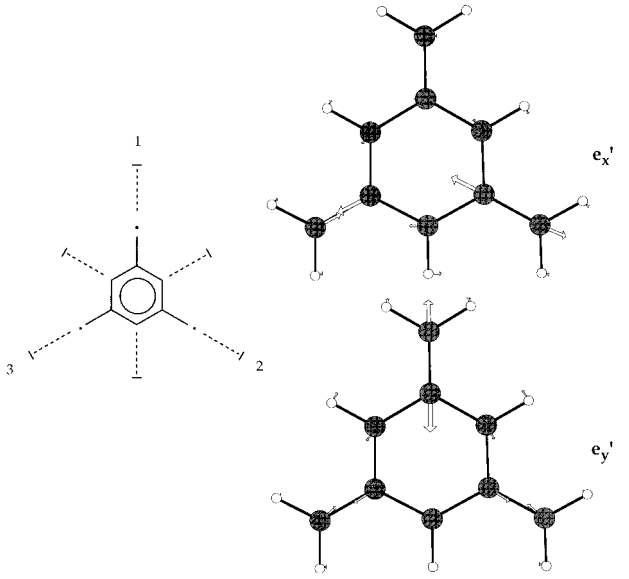

Figure 3. The three C_2 axes of **1**, labeled 1, 2, and 3 (left), and a pair of Jahn−Teller active e′ vibrational modes (right). The e_y' mode is responsible for distortion from D_{3h} to C_{2v} symmetry, maintaining the C_2 axis labeled 1. Mixing of the e_y' with the e_x' mode allows distortion to the equivalent C_{2v} structures, where the C_2 axis labeled 2 or 3 is the one that is maintained.

pseudorotation pathway, and the three equivalent C_{2v} structures of the other type are expected to be the transition states that connect them.[21]

Anion $\mathbf{1}^-$ has four electrons in the three NBMOs and is thus a diradical. As shown in Figure 5, there are three configurations with $S_z = 1$ and nine configurations with $S_z = 0$. The three $S_z = 1$ configurations give rise to three triplet states, one of $^3A_2'$ symmetry and a pair that together have $^3E'$ symmetry. Each of these states also has an equivalent set of configurations for which $S_z = 0$. Since, as noted above, the NBMOs of $\mathbf{1}^-$ are nondisjoint, $\mathbf{1}^-$ should obey Hund's rule;[2,18] and one of these triplets is expected to be the ground state.

Like the $^2E''$ states of **1**, the $^3E'$ state of $\mathbf{1}^-$ should undergo a first-order Jahn−Teller distortion away from D_{3h} symmetry. In contrast, there is no *a priori* reason to believe that either the presumed $^4A_1''$ ground state of **1** or the $^3A_2'$ state of $\mathbf{1}^-$ is likely to distort away from a D_{3h} geometry. Whether the ground state of $\mathbf{1}^-$ has the same or different molecular symmetry from the ground state of **1** will affect the vibrational structure that appears in the lowest energy band of the photoelectron spectrum of $\mathbf{1}^-$.[7] Therefore, predicting correctly which triplet, $^3E'$ or $^3A_2'$, is the ground state of $\mathbf{1}^-$ is important for predicting the type of vibrational structure that should appear in this band.

Of the nine $S_z = 0$ configurations in Figure 5, the first three (d, e, and f) are obviously singlets. Configuration d is $^1A_1'$, as is the linear combination with a positive sign of configurations e and f. The combination of e and f with a negative sign is $^1E_y'$.

The remaining six $S_z = 0$ configurations in Figure 5 can be grouped into three pairs in which the two configurations that constitute each pair differ only by the exchange of α and β spin electrons between the two singly occupied NBMOs. The positive linear combination of each pair is the $S_z = 0$ component of a triplet, either $^3A_2'$ or $^3E'$. In the former triplet state, a_2'' is doubly occupied and the two e″ NBMOs are each singly occupied (configurations g + h). In the latter triplet state, three electrons occupy the e″ NBMOs [configurations i + j and k + l).

The negative combination of configurations g and h, in which one electron resides in each e″ NBMO, is $1\ ^1E_x'$. It is the complement to the $1\ ^1E_y'$ state, comprised of configurations e and f. In the second $^1E'$ pair of states, the a_2'' NBMO is singly occupied and three remaining electrons occupy the e″ orbitals. These $2\ ^1E'$ states involve negative linear combinations of the configurations, i − j for $2\ ^1E_y'$ and k − l for $2\ ^1E_x'$.

Since, as shown in Figure 5, each singlet state involves at least two configurations, it is clear that for $\mathbf{1}^-$, as for **1**, multiconfigurational wave functions must be used. Like the $^2E''$ states of **1**, the two different $^1E'$ states of $\mathbf{1}^-$ should both be unstable toward first-order Jahn−Teller distortions from D_{3h} symmetry, as should the $^3E'$ state. However, in $\mathbf{1}^-$, as in other diradicals,[2] second-order Jahn−Teller effects, involving distortions that mix states of different D_{3h} symmetries,[21] are also likely to be important.

(21) Davidson, E. R.; Borden, W. T. *J. Phys. Chem.* **1983**, *87*, 4783.

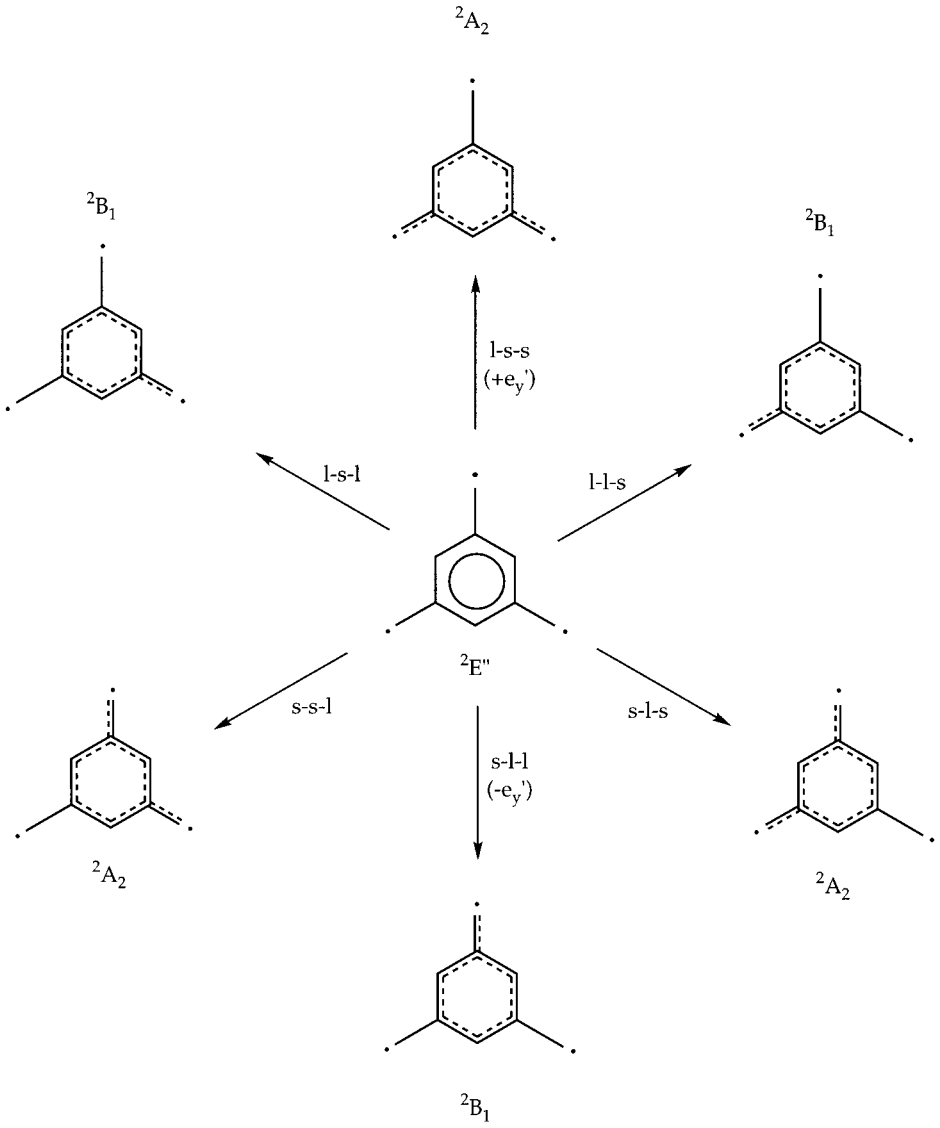

Figure 4. Schematic depiction of the $^2B_1$ and $^2A_2$ states of **1** that result from six possible e′ distortions from the D_{3h} geometry of $^2E''$. Pseudorotation interconverts the C_{2v} doublet states in a potential well around the D_{3h} $^2E''$ mountain top.

Computational Methods

CASSCF calculations were performed on the low-lying electronic states of **1** and **1**$^-$. These calculations correlated the nine π electrons in **1** and the ten π electrons in **1**$^-$ with wave functions that were comprised of all possible symmetry-adapted configurations which result from distributing the π electrons among the three bonding, three nonbonding, and three antibonding π MOs of **1** and **1**$^-$. The notation (9,9)CASSCF and (10,9)CASSCF will be used to express the number of correlated electrons and orbitals in the active space. Calculations were performed with the 6-31G* and 6-31+G* basis sets.[22] The CASSCF calculations were carried out with the MOLCAS v.3 suite of *ab initio* programs.[23]

In performing calculations at D_{3h} geometries, MOLCAS v.3 does not make use of the full D_{3h} point group but instead, utilizes only the C_{2v} subgroup. The a_1'' and e_x'' representations of D_{3h} both belong to the a_2 representation of the C_{2v} subgroup, and a_2'' and e_y'' of D_{3h} both belong to b_1 of C_{2v}. Artifactual symmetry breaking in the wave functions for **1** and **1**$^-$ at D_{3h} geometries can thus lead to MOs and states that are mixtures of two different D_{3h} representations.[21] Therefore, unless precautions are taken to avoid artifactual symmetry breaking, orbitals and electronic states of **1** and **1**$^-$ should really be designated by their C_{2v}, rather than D_{3h}, symmetry labels.

It was possible to perform the CASSCF calculations on **1** and **1**$^-$ at D_{3h} geometries with D_{3h} symmetry imposed upon the π MOs. Since the $^4A_1''$ state of **1** belongs to the totally symmetric representation of D_{3h}, each of the CASSCF MOs for this state was expected to be of pure D_{3h} symmetry; this was, in fact, found to be the case. These MOs were used to start CASSCF calculations on other electronic states of **1** in D_{3h} symmetry. In order to keep the a_2'' and e_y'' MOs from mixing in the course of the CASSCF calculations, the SUPSYM option in the RASSCF module of MOLCAS v.3 was used. All of the D_{3h} calculations on **1** were performed at the optimized geometry of $^4A_1''$.

Similarly, calculations on the electronic states of **1**$^-$ in D_{3h} symmetry were performed at the optimized geometry of $^1A_1'$. The pure D_{3h} symmetry MOs of this state were used as an initial guess, and the SUPSYM option was employed to maintain the D_{3h} symmetry of the π MOs during the CASSCF calculations.

C_{2v} geometries were optimized at the (9,9)CASSCF/6-31G* level for the low-lying electronic states of **1** and at the (10,9)CASSCF/6-31G* and (10,9)CASSCF/6-31+G* levels for the low-lying electronic states of **1**$^-$. It was not possible to perform vibrational analyses at the geometries optimized with these CASSCF wave functions, since MOLCAS v.3 does not have a module for obtaining analytical second derivatives; these CASSCF calculations were too big to be handled by Gaussian 94.

(22) (a) Hariharan, P. C.; Pople, J. A. *Theor. Chim. Acta* **1973**, *28*, 213. (b) Clark, T.; Chandrasekhar, J.; Spitznagel, G. W.; Schleyer, P. v. R. *J. Comput. Chem.* **1983**, *4*, 294.

(23) MOLCAS, version 3; Andersson, K.; Blomberg, M. R. A.; Fülscher, M. P.; Kellö, V.; Lindh, R.; Malmqvist, P.-Å.; Noga, J.; Olsen, J.; Roos, B. O.; Sadlej, A. J.; Siegbahn, P. E. M.; Urban, M.; Widmark, P.-O.; University of Lund, Sweden 1994.

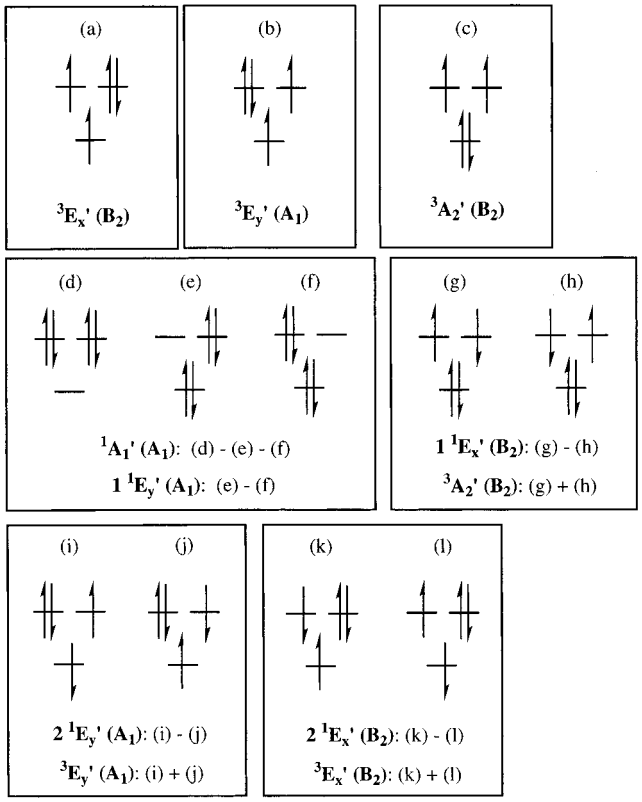

Figure 5. $S_z = 1$ (a−c) and $S_z = 0$ (d−l) configurations for the D_{3h} states of $\mathbf{1}^-$. C_{2v} symmetries are given in parentheses.

Gaussian 94[24] was used to perform smaller calculations to investigate the size of the zero-point correction to the energy difference between the $^4A_1''$, $1\ ^2B_1$, and $1\ ^2A_2$ states of **1**. Since a single configuration is dominant in the (9,9)CASSCF wave function for $^4A_1''$, the D_{3h} equilibrium geometry of this state was reoptimized and a vibrational analysis performed at the ROHF/3-21G level of theory. Since several configurations with differing occupations of the three NBMOs (Figure 2) are important in the wave functions for $1\ ^2B_1$ and $1\ ^2A_2$, their C_{2v} optimized geometries were reoptimized and vibrational analyses performed at the (3,3)CASSCF/3-21G level of theory.

Gaussian 94 was also used to carry out unrestricted (U)B3LYP/6-31+G* calculations on the lowest states of **1** and $\mathbf{1}^-$. B3LYP is a hybrid density functional method that uses three parameter exchange functional of Becke[25] and the nonlocal correlation functional of Lee, Yang, and Parr.[26] The UB3LYP/6-31+G* calculations were used to calculate the electron affinity and vibrational frequencies of $^4A_1''$. For comparison, UB3LYP/6-31+G* geometry optimizations and frequency calculations were also performed on benzyl radical and benzyl anion.

The effects of dynamic electron correlation[27] between σ and π electrons in **1** and $\mathbf{1}^-$ were taken into account by performing single-point calculations at the CASSCF/6-31G*-optimized geometries. Two different computational methods were employed. One method, CASPT2N,[28] used second-order perturbation theory to provide additional correlation for the CASSCF wave function. The CASPT2N calculations were performed with MOLCAS v.3.[23]

The other method used multireference configuration interaction (MR-CI) calculations to provide $\sigma-\pi$ correlation. Configurations were generated by allowing simultaneous single excitations in both the σ and π spaces, as well double excitations in the π space, from several reference configurations. Energy corrections for neglected quadruple excitations were made using the Davidson formula.[29] These CI calculations are abbreviated MR-CI(π-SD,σ-S)+Q and were performed with the MELDF-X suite of programs.[30]

Canonical CASSCF MOs were used for these CI calculations, and the MOs were imported into MELDF-X from MOLCAS. The reference space for each electronic state was comprised of the most important configurations from the CASSCF calculations. The reference configurations used for the MR-CI calculations are given in Tables 1 and 2. The cumulative weights (Σc^2) of these configurations accounted for about 80% of the CASSCF wave functions, except in for the doublet states of **1**.

Configurations a and b in Figure 2 are by far the biggest contributors to the $1\ ^2E_y''$ CASSCF wave function for **1**, and c and d are the most important configurations in the CASSCF wave function for $1\ ^2E_x''$. However, for each component of $1\ ^2E''$, these two reference configurations represent less than 70% of the total CASSCF wave function. In order to make the weights of the reference configurations for $1\ ^2E''$ comparable to those for the other states of **1**, additional configurations were added to the CI reference space for each component of $1\ ^2E''$: e and f for $1\ ^2E_y''$ and g and h for $1\ ^2E_x''$.[31]

In some of our MR-CI(π-SD,σ-S) calculations, files were created that were too large (>2 GB) to handle. In those cases, second-order perturbation theory was used to eliminate configurations that contributed less than a fixed threshold energy, typically 10^{-7} hartree. The threshold was chosen such that only $0.20 \pm 0.05\%$ of the correlation energy, predicted by perturbation theory, was discarded. The MR-CI(π-SD,σ-S) energy was corrected for the percentage of the correlation lost. Test calculations showed that this procedure affects the relative energies of different states by less than 0.1 kcal/mol.

Results and Discussion

Calculated CASSCF, CASPT2N, and MR-CI(π-SD,σ-S)+Q energies for the low-lying electronic states of **1** at both D_{3h} and C_{2v} geometries are listed in Table 1 and shown schematically in Figure 6. The same information for $\mathbf{1}^-$ is provided in Table 2 and Figure 7. Table 3 provides the CASSCF/6-31G*-optimized geometries of these states, using the atom-numbering scheme in Figure 8.

Calculations on 1 at D_{3h} Geometries. As expected, the electronic state of lowest energy for **1** is $^4A_1''$. The first excited state, $1\ ^2E''$, is computed to lie 18.3 kcal/mol higher in energy than $^4A_1''$ at the CASSCF level of theory. Maintaining pure D_{3h} symmetry for the CASSCF MOs, using the method

(24) Gaussian 94, revision B.3; Frisch, M. J.; Trucks, G. W.; Schlegel, H. B.; Gill, P. M. W.; Johnson, B. G.; Robb, M. A.; Cheeseman, J. R.; Keith, T.; Petersson, G. A.; Montgomery, J. A.; Raghavachari, K.; Al-Laham, M. A.; Zakrzewski, V. G.; Ortiz, J. V.; Foresman, J. B.; Peng, C. Y.; Ayala, P. Y.; Chen, W.; Wong, M. W.; Andres, J. L.; Replogle, E. S.; Gomperts, R.; Martin, R. L.; Fox, D. J.; Binkley, J. S.; Defrees, D. J.; Baker, J.; Stewart, J. P.; Head-Gordon, M.; Gonzalez, C.; Pople, J. A.; Gaussian, Inc.: Pittsburgh, PA, 1995.

(25) Becke, A. D. *J. Chem. Phys.* **1993**, *98*, 5648.

(26) Lee, C.; Yang, W.; Parr, R. G. *Phys. Rev. B* **1988**, *37*, 785.

(27) For a review, see: Borden, W. T.; Davidson, E. R. *Acc. Chem. Res.* **1996**, *29*, 67.

(28) Andersson, K.; Malmqvist, P.-Å.; Roos, B. O. *J. Chem. Phys.* **1992**, *96*, 1218.

(29) Davidson, E. R. In *The World of Quantum Chemistry*; Daudel, R., Pullman, B., Eds.; D. Reidel: Dordrecht, The Netherlands, 1974.

(30) MELDF-X was originally written by L. McMurchie, S. Elbert, S. Langhoff, and E. R. Davidson. It has been substantially modified by D. Feller, R. Cave, D. Rawlings, R. Frey, R. Daasch, L. Nitchie, P. Phillips, K. Iberle, C. Jackels, and E. R. Davidson.

(31) Because MELDF-X allows one to specify only the occupation numbers of the MOs, but not the spin coupling in reference configurations, addition of configurations g and h to the reference space for $1\ ^2E_x''$ meant that configuration i was also added. Configuration i for the three electrons in the NBMOs, when coupled to the lowest energy closed-shell wave function for the rest of the electrons in **1**, contributes to a $^2A_1''$ state and to the $S_z = {}^1/_2$ component of $^4A_1''$. Therefore, configuration i cannot contribute to the $1\ ^2E_x''$ wave function. Thus, the presence of configuration i in the reference space for this component of $1\ ^2E''$ might appear to be without consequence. However, excitations of electrons from doubly occupied to unoccupied MOs in **1** can have E_x' symmetry. These excitations, when coupled to configuration i, give excited configurations that are $^2E_x''$ and which have no counterparts in the excited $^2E_y''$ configurations, as generated from reference configurations e and f. Consequently, because configuration i has A_1'' symmetry, the addition of it to the reference space for $1\ ^2E_x''$ results in artifactual symmetry breaking and leads to the expectation that the MR-CI(π-SD,σ-S) wave function for $1\ ^2E_x''$ will have lower energy than the MR-CI(π-SD,σ-S) wave function for $1\ ^2E_y''$.

Table 1. Absolute (hartrees) and Relative (kcal/mol) Energies for **1** with the 6-31G* Basis Set

			absolute energies[a]				relative energies[b]			
state	geometry	configs[c]	CAS[d]	CASPT2N	MCSCF ref[e]	CI[f]	CI (pert)[g]	CAS	CASPT2N	CI+Q[h]
$^4A_1''$	D_{3h}	g + h + i	−1.043 314	−2.113 37	−0.928 22	−1.381 907	−1.381 12	0.0	0.0	0.0
1 $^2B_1$	C_{2v}	a − b	−1.018 043	−2.091 52	−0.886 93		−1.350 37	15.9	13.7	16.5
1 $^2A_2$	C_{2v}	c − d	−1.018 284	−2.091 38	−0.889 29		−1.352 58	15.7	13.8	14.7
1 $^2E_y''$ (B_1)	D_{3h}	a − b	−1.014 114	−2.090 69	−0.870 88		−1.342 07	18.3	14.2	19.2
1 $^2E_x''$ (A_2)	D_{3h}	c − d	−1.014 115	−2.090 69	−0.871 39		−1.343 69	18.3	14.2	17.2
2 $^2B_1$	C_{2v}	e − f	−0.985 873	−2.066 88				36.0	29.2	
2 $^2A_2$	C_{2v}	g − h	−0.987 587	−2.063 14				35.0	31.5	
2 $^2E_y''$ (B_1)	D_{3h}	e − f	−0.982 899	−2.066 44				37.9	29.4	
2 $^2E_x''$ (A_2)	D_{3h}	g − h	−0.982 896	−2.066 42				37.9	29.5	
$^2A_1''$ (A_2)	D_{3h}	g + h − i	−0.952 205	−2.036 37				57.2	48.3	
$^2A_2''$ (B_1)	D_{3h}	e + f	−0.865 403	−2.013 28				111.6	62.8	

[a] Absolute energies +345 hartrees. [b] Relative to $^4A_1''$ state. [c] Principle configurations and signs (as shown in Figure 2). [d] (9,9)CASSCF. [e] Energy of the zeroth-order reference space for MR-CI(π-SD,σ-S) calculations. [f] MR-CI(π-SD,σ-S). [g] Using perturbational truncation of the MR-CI(π-SD,σ-S) configuration list (see Computational Methods). [h] Relative energies including the Davidson correction.

Table 2. Absolute (hartrees) and Relative (kcal/mol) Energies for $\mathbf{1}^-$ with the 6-31G* Basis Set

			absolute energies[a]				relative energies[b]			
state	geometry	configs[c]	CAS[d]	CASPT2N	MCSCF ref[e]	CI[f]	CI (pert)[g]	CAS	CASPT2N	CI+Q[h]
$^3B_2$	C_{2v}	a	−0.983 820	−2.097 98	−0.884 86	−1.358 466	−1.357 86	0.0	0.0	0.0
$^3A_1$	C_{2v}	b	−0.981 643	−2.097 75	−0.878 42	−1.354 274		1.4	0.1	1.5
$^3E_y'$ (A_1)	D_{3h}	b	−0.977 562	−2.097 23	−0.867 39	−1.348 437		3.9	0.5	3.6
$^3E_x'$ (B_2)	D_{3h}	a (+ c)[i]	−0.978 007	−2.096 71	−0.859 73	−1.345 955		3.6	0.8	3.9
$^3E_x'$ (B_2 av)[j]	D_{3h}	a	−0.975 459	−2.099 52	−0.865 08	−1.347 805		5.2	−1.0	3.7
$^3A_2'$ (B_2 av)[j]	D_{3h}	c	−0.967 872	−2.098 35	−0.850 20	−1.340 499		10.0	−0.2	6.4
$^1A_1'$	D_{3h}	d − e − f	−0.975 909	−2.098 29	−0.856 05		−1.342 50	5.0	−0.2	6.1
$^1A_1$ (l-s-s)	C_{2v}	d − f	−0.977 568	−2.094 07	−0.859 44	−1.341 512	−1.340 88	3.9	2.4	7.8
$^1A_1$ (s-l-l)	C_{2v}	d − e	−0.977 839	−2.093 91	−0.869 68	−1.347 236		3.8	2.6	5.9
$^1B_2$	C_{2v}	g − h	−0.958 224	−2.076 83				16.1	13.3	
$^1A_1$	C_{2v}	e − f	−0.956 178	−2.082 21				17.3	9.9	
1 $^1E_x'$ (B_2)	D_{3h}	g − h	−0.951 021	−2.083 68				20.6	9.0	
1 $^1E_y'$ (A_1)	D_{3h}	e − f	−0.950 966	−2.083 89				20.6	8.8	
2 $^1E_y'$ (A_1)	D_{3h}	i − j	−0.911 115	−2.047 79				45.6	31.5	
2 $^1E_x'$ (B_2)	D_{3h}	k − l	−0.911 281	−2.047 58				45.5	31.6	

[a] Absolute energies +345 hartrees. [b] Relative to $^3B_2$ state. [c] Principle configurations and signs (as shown in Figure 5). [d] (10,9)CASSCF. [e] Energy of the zeroth order reference space for MR-CI(π-SD,σ-S) calculations. [f] MR-CI(π-SD,σ-S). [g] Using perturbational truncation of the MR-CI(π-SD,σ-S) configuration list (see Computational Methods). [h] Relative energies including the Davidson correction. [i] See text for discussion of $^3A_2'$ contaminant. [j] Using orbitals optimized for both the first and second B_2 roots ($^3E'$ and $^3A_2'$). See text for details.

described in the preceding section, gives identical energies for 1 $^2E_x''$ and 1 $^2E_y''$ at both the CASSCF and CASPT2N levels of theory.

When CASSCF calculations were performed on 1 $^2E''$ at the same D_{3h} geometry,[32] but without enforcing D_{3h} symmetry on the CASSCF wave functions, the energies obtained for the two lowest doublet states ($^2B_1$ and $^2A_2$ in C_{2v} symmetry) were each only 0.2 kcal/mol lower than those calculated for the pure $^2E''$ states. This shows that there is very little artifactual symmetry breaking in the C_{2v} CASSCF $^2B_1$ and $^2A_2$ wave functions, since their energies are nearly the same as the pure 1 $^2E''$ wave functions at the same D_{3h} geometry.

At this geometry, CASPT2N calculations with the D_{3h} CASSCF MOs gave an energy for 1 $^2E''$ that is 14.2 kcal/mol higher than that for $^4A_1''$. Using the CASSCF MOs on which only C_{2v} symmetry was imposed, the CASPT2N energies of $^2B_1$ and $^2A_2$ were both 0.4 kcal/mol *higher* than that of 1 $^2E''$, calculated with CASSCF MOs of pure D_{3h} symmetry.

Identical energies for each component of 1 $^2E''$ were obtained by the MR-CI(π-SD,σ-S)+Q calculations when a two-configuration reference space was used: a and b for 1 $^2E_y''$ and c and d for 1 $^2E_x''$. However, as discussed in the previous section, these two pairs of configurations constitute less than 70% of the CASSCF wave function for each component of 1 $^2E''$; whereas, the reference configuration for the MR-CI(π-SD,σ-S)+Q calculation on $^4A_1''$ constitutes 80% of the CASSCF wave function for this state. Having ca. 10% less of the CASSCF wave function in the reference space for 1 $^2E''$ leads to its MR-CI(π-SD,σ-S)+Q energy being calculated too high, relative to that of $^4A_1''$.

When configurations e and f are added to the reference space for 1 $^2E_y''$ and configurations g and h are added to the reference space for 1 $^2E_x''$, the reference configurations constitute a percentage of the CASSCF wave function for each of the two components of 1 $^2E''$ that is more comparable to the percentage for $^4A_1''$. However, this increase in the percentage of the CASSCF wave function in the reference space for 1 $^2E_y''$ and 1 $^2E_x''$ was achieved only at the expense of contaminating the reference space for 1 $^2E_x''$ with a configuration i, which has $^2A_1''$ symmetry.[31] As expected, the presence of configuration i in the reference space for 1 $^2E_x''$ results in the MR-CI(π-SD,σ-S)+Q energy for this wave function being significantly lower than that for 1 $^2E_y''$. The difference in the two MR-CI(π-SD,σ-S)+Q energies, for what should be the two degenerate components of 1 $^2E''$, amounts to 2 kcal/mol. Which MR-CI(π-SD,σ-S)+Q energy for 1 $^2E''$ should be compared with the $^4A_1''$ energy?

The answer becomes clear when it is noted that the additional reference configurations in the 1 $^2E_x''$ calculation are the same as those in the $^4A_1''$ calculation.[33] Since 1 $^2E_x''$ is treated in a manner which is equivalent to $^4A_1''$ in the MR-CI(π-SD,σ-S)+Q calculations, the relative energies of these two states should be reliable.

(32) Geometry optimization of 1 $^2E''$ within the D_{3h} point group gave an energy 0.3 kcal/mol lower than that calculated for 1 $^2E''$ at the D_{3h} geometry of $^4A_1''$.

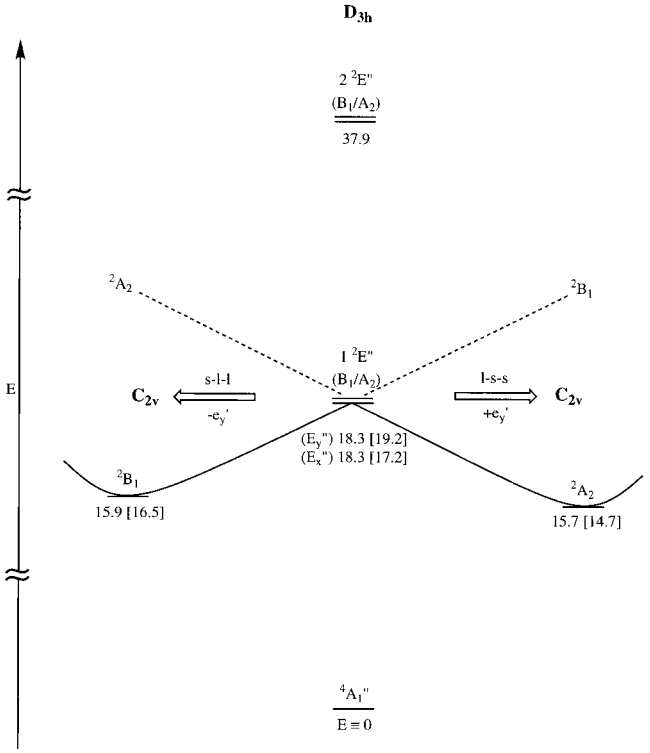

Figure 6. Schematic depiction of the relative energies of the electronic states of **1**. The relative energies, calculated at CASSCF and [MR-CI(π-SD,σ-S)+Q] levels, in kcal/mol are also given. The D_{3h} states are shown in the center and the C_{2v} states are on the sides. As noted in the text, the MR-CI energy of 1 $^2E_y''$, which should be the same as that of 1 $^2E_x''$, is spuriously computed to be too high by 2.0 kcal/mol. This leads to the MR-CI energy of the Jahn−Teller distorted C_{2v} geometry of 1 $^2E_y''$ ($^2A_2$) being computed to be too high by the same amount.

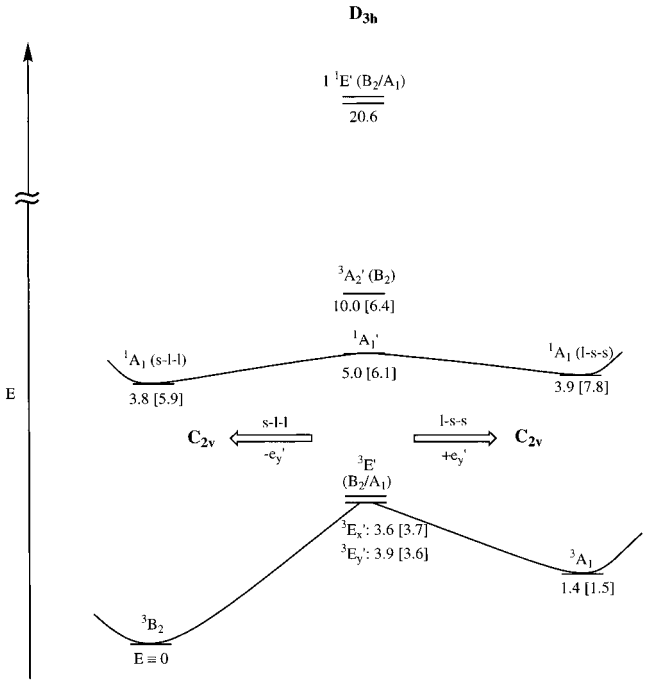

Figure 7. Schematic depiction of the relative energies of electronic states of $\mathbf{1}^-$. The relative energies calculated at CASSCF and [MR-CI(π-SD,σ-S)+Q] levels in kcal/mol are also given. The D_{3h} states are shown in the center and the C_{2v} states are on the sides.

Calculations of energy separations between electronic states of different spin in other molecules[16] find that MR-CI(π-SD,σ-S)+Q energy differences usually fall in between those computed at the CASSCF and CASPT2N levels.[34] The fact that this is the case for the MR-CI(π-SD,σ-S)+Q energy separation between $^4A_1''$ and 1 $^2E_x''$, but not 1 $^2E_y''$, provides additional evidence that it is the former energy difference which is likely to be accurate.

Another $^2E''$ state, 2 $^2E''$, whose dominant configurations are e and f for the 2 $^2E_y''$ component and g and h for the 2 $^2E_x''$ component, is calculated to be the second excited state. It is higher in energy than the first excited state, because in the 1 $^2E''$ state one of the two configurations (a in 1 $^2E_y''$ and c in 1 $^2E_x''$) has all three electrons in the degenerate pair of e″ NBMOs. In contrast, both of the important configurations in each component of 2 $^2E''$ have one electron in the nondegenerate a_2'' NBMO. This difference between the two $^2E''$ states is responsible for their energy ordering.

The reason why this is the case can be seen by inspection of the NBMOs in Figure 1. It shows that e_x'' and e_y'' are more disjoint than are a_2'' and either of the e″ NBMOs. For example, e_x'' has coefficients only at carbons where e_y'' has small coefficients but at two carbons where a_2'' has large coefficients. Consequently, an electron in e_x'' and one of opposite spin in e_y'' have a lower probability of occupying the same p−π AO simultaneously and, thus, have a lower Coulombic repulsion energy than electrons of opposite spin in a_2'' and either of the e″ NBMOs.

In 2 $^2E''$, the electron in a_2'' has the same spin as one of the electrons in e″; the Pauli principle prevents these two electrons of the same spin from simultaneously appearing in the same AO. In contrast, in the $^2A_1''$ state the electrons in the e″ NBMOs have the same spin as each other, but the opposite spin from the electron in the a_2'' NBMO. Thus, in $^2A_1''$ the electrons in the e″ NBMOs are prevented from simultaneously appearing in the same AO, but neither of the electrons in e″ is prevented from appearing in the same AO as the electron in a_2''.

As noted above, e_x'' and e_y'' are more disjoint than are a_2'' and either of the e″ NBMOs. Consequently, preventing the electrons in the e″ NBMOs from appearing in the same AO has a smaller effect on reducing the Coulombic repulsion than preventing one of the electrons in e″ and the electron in a_2'' from appearing in the same AO. Therefore, $^2A_1''$ should lie well above 2 $^2E_y''$, as is the case.

Finally, in $^2A_2''$ two electrons occupy the same e″ NBMO; but, in contrast to those in 2 $^2E_y''$, they are anticorrelated. Therefore, $^2A_2''$ has a highly ionic π wave function, which should give it a high energy but allow it to be strongly stabilized by inclusion of $\sigma-\pi$ correlation. The results in Table 1 confirm both of these expectations.

Calculations on 1 at C_{2v} Geometries. The Jahn−Teller theorem predicts that the 1 $^2E''$ and 2 $^2E''$ states of **1** will undergo a geometrical distortion away from D_{3h} symmetry and that the energy lowering will, at least for small distortions, be linear in the distortion coordinate.[20] These molecular distortions occur because, at D_{3h} geometries, single excitations of the type $a_2'' \leftrightarrow e_y''$, involving one NBMO and either a bonding or antibonding MO, generate configurations that have $^2E''$ symmetry but

(33) Implicit inclusion of E_x'' configurations in the $^4A_1''$ reference space, where each NBMO is singly occupied (g, h, and i), can affect the wave function in the same way as has been described for $^2E_x''$.[31] Excitations of electrons from doubly occupied to unoccupied MOs in **1** can have E_x' symmetry. These excitations, when coupled to E_x'' configurations for the three electrons in the NBMOs, give excited configurations that are $^4A_1''$.

(34) CASSCF calculations do not include any dynamic correlation between σ and π electrons; CASPT2N, by using second-order perturbation theory, exaggerates the effect of dynamic correlation. A CI calculation in which the magnitude of the energy difference between two spin states is correctly computed should thus give an energy separation whose size is intermediate between that computed at the CASSCF and CASPT2N levels.

Table 3. CASSCF[a]/6-31G*-Optimized Geometries for Important States of **1** and $\mathbf{1}^-$

	1			$\mathbf{1}^-$				
	$^4A_1''$	$^2B_1$	$^2A_2$	$^3B_2$	$^3A_1$	$^1A_1'$	$^1A_1$ (l-s-s)	$^1A_1$ (s-l-l)
				Distances[b]				
C5−C1	1.403	1.397	1.469	1.384	1.439	1.415	1.451	1.379
C6−C3	1.403	1.446	1.410	1.424	1.394	1.415	1.396	1.437
C1−C2	1.424	1.430	1.399	1.442	1.407	1.422	1.403	1.447
C2−C3	1.424	1.396	1.432	1.410	1.434	1.422	1.441	1.403
C3−C4	1.424	1.419	1.413	1.418	1.435	1.422	1.428	1.418
H7−C5	1.074	1.074	1.072	1.078	1.076	1.076	1.075	1.078
H8−C6	1.074	1.073	1.073	1.076	1.077	1.076	1.077	1.075
H9−C6	1.074	1.073	1.073	1.076	1.077	1.076	1.077	1.076
H10−C2	1.075	1.076	1.076	1.080	1.079	1.079	1.079	1.080
H11−C4	1.075	1.075	1.076	1.077	1.079	1.079	1.080	1.078
				Angles[c]				
C2−C1−C2′	118.1	117.5	119.2	113.5	122.0	118.6	122.0	114.4
C1−C2−C3	121.9	121.8	121.6	123.9	120.5	121.4	120.4	123.0
C2−C3−C4	118.1	118.7	117.9	119.9	116.5	118.6	116.5	120.3
C3−C4−C3′	121.9	121.4	122.0	119.0	124.1	121.4	124.2	119.0
C6−C3−C4	121.0	120.4	121.2	119.2	119.0	120.7	119.3	121.8

[a] (9,9)CASSCF for **1** and (10,9)CASSCF for $\mathbf{1}^-$. [b] Bond distances are in angstroms. [c] Bond angles are in degrees.

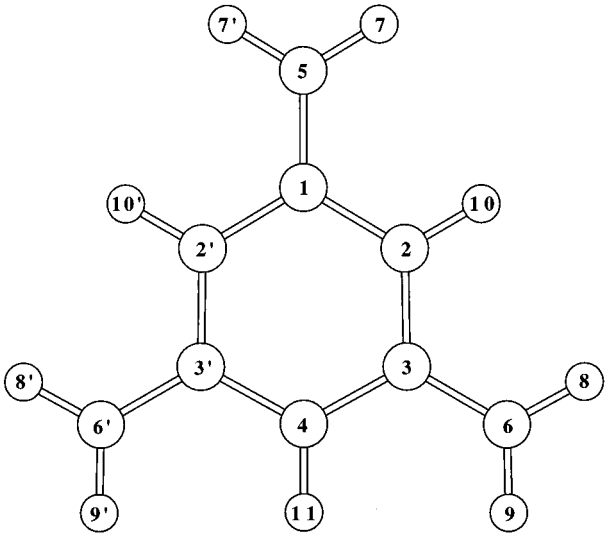

Figure 8. Atom numbering for geometries reported in Table 3.

which effectively allow orbitals of a_2'' and e_y'' symmetry to mix. This mixing reduces the Coulombic repulsion between electrons of opposite spin by increasing the degree to which the orbitals that these electrons occupy are disjoint.[2,18] However, it also has the effect of reducing the effective symmetry of the bonding MOs from pure D_{3h} to C_{2v}, and it is this distortion of the symmetry of the π bonding MOs that is largely responsible for the molecular distortion that is predicted by the Jahn−Teller theorem.[20,21]

Since the lowest energy doublet state (1 $^2E''$) is subject to first-order Jahn−Teller distortions, the doublet−quartet splitting in **1** will be determined by the energy of the C_{2v} minima on the potential surface for pseudorotation in the lowest doublet state, relative to that of the D_{3h} equilibrium geometry of the $^4A_1''$ state (see Figure 6). The CASSCF and the MR-CI(π-SD,σ-S)+Q calculations both predict an energy lowering of about 2.5 kcal/mol upon Jahn−Teller distortions of $^2E''$, with both the $^2E_x''$ ($^2A_2$) and $^2E_y''$ ($^2B_1$) components being stabilized to about the same extent.

The $^2E_x''$ component of $^2E''$ is stabilized by distortions that lengthen the C−C bond to one methylene group and shorten the C−C bonds to the other two. The resulting $^2A_2$ geometries and wave functions are similar to those of triplet *m*-benzoquinodimethane,[15] plus an electron in an isolated p orbital. For the $^2E_y''$ component, an energy lowering is found for distortions that shorten one methylene C−C bond and lengthen the other two. The resulting $^2B_1$ structures and wave functions are similar to those of benzyl radical, plus an electron largely localized in each of the p orbitals on the two remaining methylene carbons, as in the $^1A_1$ state of *m*-benzoquinodimethane.[15]

The nearly equal stabilization of both components of $^2E''$ indicates that these energy lowerings are largely first-order and do not involve appreciable second-order Jahn−Teller effects. The latter would have led to energetically significant local minima and maxima (transition states) along the coordinate for pseudorotation between distorted geometries with $^2E_x''$ ($^2A_2$) and $^2E_y''$ ($^2B_1$) wave functions.[2,21] However, our calculations indicate that pseudorotation in the lowest doublet state of **1** does not involve any significant energy barriers.

The CASPT2N calculations predict an energy lowering of $^2E''$ upon Jahn−Teller distortions of only ca. 0.5 kcal/mol, just 20% of that computed at the CASSCF and the MR-CI(π-SD,σ-S)+Q levels. Since CASPT2N uses second-order perturbation theory, it tends to overestimate the extent to which dynamic correlation between the σ and π electrons stabilizes ionic terms in π wave functions. For example, this overestimation is responsible for the finding that the CASPT2N D_{3h} energy difference between $^4A_1''$ and 1 $^2E''$ is 3.0 kcal/mol smaller than this energy difference at the MR-CI(π-SD,σ-S)+Q level of theory.

Because CASPT2N overemphasizes the effect of $\sigma-\pi$ correlation, the mixing between a_2'' and e_y'' MOs, which reduces ionic terms in the $^2E''$ wave functions, is underestimated. Since this mixing is largely responsible for the first-order Jahn−Teller effect in **1**, CASPT2N underestimates the size of the stabilization of $^2E''$ by a first-order Jahn−Teller distortion.

The overemphasis of the effect of $\sigma-\pi$ correlation on stabilizing 1 $^2E''$ is nearly balanced by the underestimation by CASPT2N of the energy lowering upon Jahn−Teller distortion of 1 $^2E''$. Thus, CASSCF, CASPT2N, and MR-CI(π-SD,σ-S)+Q all predict values of $\Delta E_{DQ} = 14.7 \pm 1.0$ kcal/mol for the adiabatic energy difference between the $^4A_1''$ ground state and the Jahn−Teller-distorted 1 $^2E''$ first excited state of **1**. Vibrational analyses indicate that the zero-point energy of the $^4A_1''$ state is ca. 1.0 kcal/mol larger than that of the lower energy of the two C_{2v} geometries of Jahn−Teller-distorted 1 $^2E''$. Therefore, we predict $\Delta E_{DQ} = 14 \pm 1$ kcal/mol in **1**.

Calculations on 1 at Twisted C_{2v} Geometries. Although vibrational analyses on $^4A_1''$, $^2B_1$, and $^2A_2$ show real frequencies

for all out-of-plane vibrations, we performed (9,9)CASSCF/6-31G* calculations on **1** at geometries where one methylene is twisted perpendicular to the benzene ring. Twisting of a methylene group raises the energy of the quartet by 15.5 kcal/mol.[35,36] The twisted geometry and orbitals resemble those of triplet *m*-benzoquinodimethane, plus an electron of the same spin in an isolated p orbital on the twisted methylene carbon.

In contrast to the high barrier to rotation of a methylene group in the quartet state of **1**, the barrier to rotation in the "long-short-short", Jahn−Teller-distorted, 1 ^{2}E″ state (^{2}A$_2$) is calculated to be very small. The bond lengths in the twisted doublet are essentially the same as those in the planar ^{2}A$_2$ component of 1 ^{2}E″, because, as noted previously, the wave function for planar ^{2}A$_2$ resembles that for triplet *m*-benzoquinodimethane plus an electron of opposite spin in an isolated p orbital. Consequently, the twisted geometry of this doublet lies only 0.3 kcal/mol higher than the planar geometry at the CASSCF level of theory.[37]

The twisted doublet and the twisted quartet both resemble triplet *m*-benzoquinodimethane plus an electron in an isolated p orbital on the twisted methylene carbon, and the wave function for the doublet differs from that for the quartet only by inversion of the spin of the electron in the twisted p orbital. Since, the twisted p orbital is disjoint from the π orbitals, the total energies of the twisted doublet and twisted quartet states are nearly the same, differing by only 0.5 kcal/mol at the CASSCF level of theory.

Calculations on $\mathbf{1}^-$ at D_{3h} Geometries. As shown in Table 2 and Figure 7, at both the CASSCF and MR-CI(π-SD,σ-S)+Q levels, the ^{3}E′ state of D_{3h} $\mathbf{1}^-$ is calculated to lie below the ^{1}A$_1$′ state, but only by a little more than 1 kcal/mol at the CASSCF level and 2 kcal/mol at the MR-CI(π-SD,σ-S)+Q level. At the CASPT2N level, the energy ordering is actually reversed, and ^{1}A$_1$′ is calculated to lie about 1 kcal/mol below ^{3}E′.

The finding that ^{3}E′ and ^{1}A$_1$′ have very similar energies is rather surprising. The dominant configuration ($c^2 = 0.47$) in the CASSCF wave function for the ^{1}A$_1$ state is d of Figure 5, in which the four electrons in the NBMOs of $\mathbf{1}^-$ all occupy the degenerate e″ NBMOs. Removing one of these electrons from e″ and placing it in the a$_2$″ NBMO with opposite spin to form the dominant configurations (a and b) for each component of the ^{3}E′ state might have been expected to provide significant stabilization for ^{3}E′. On going from ^{1}A$_1$′ to ^{3}E′, the Coulombic repulsion associated with having two electrons of opposite spin in the same e″ NBMO is replaced by the much smaller repulsion associated with having two electrons with parallel spins, one in the a$_2$″ NBMO and the other in one of the e″ NBMOs.

Three factors provide stabilization for ^{1}A$_1$′, relative to ^{3}E′. One is the presence of configurations e and f in the wave function for ^{1}A$_1$′. Each of these configurations ($c^2 = 0.15$) provides correlation between the pair of electrons that occupy one of the e″ NBMOs in configuration d.

Another factor which stabilizes ^{1}A$_1$′ relative to ^{3}E′ is that, in the triplet, the electron that occupies the a$_2$″ NBMO and one of the electrons in the e″ NBMOs have opposite spin. In the singlet, this pair of electrons with opposite spin occupy the e$_x$″ and e$_y$″ NBMOs. As discussed in the previous section, the e″ pair of NBMOs is more disjoint than a$_2$″ and either e″ NBMO. Consequently, the Coulombic repulsion energy that is associated with a pair of electrons of opposite spin in the e$_x$″ and e$_y$″ NBMOs in configuration d of ^{1}A$_1$′ is smaller than that associated with the electrons of opposite spin in the a$_2$″ and e″ NBMOs in configurations a or b of ^{3}E′.

Finally, dynamic correlation between the four π electrons in the NBMOs and the six electrons in the bonding π MOs of $\mathbf{1}^-$ also stabilizes ^{1}A$_1$′, relative to ^{3}E′. This is evident from the fact that (4,3)CASSCF places ^{3}E′ 12 kcal/mol lower than ^{1}A$_1$′, but that (10,9)CASSCF reduces this energy difference to 1 kcal/mol.

It should be noted that the ^{3}E$_x$′ CASSCF wave function for $\mathbf{1}^-$ has a ^{3}A$_2$′ contaminant, even when π MOs of pure D_{3h} symmetry are used and π orbitals of different symmetries are not allowed to mix. Although the most important configuration ($c^2 = 0.66$) in the ^{3}E$_x$′ CASSCF wave function is a of Figure 5, the second most important configuration ($c^2 = 0.15$) is c. The latter is a ^{3}A$_2$′, not a ^{3}E$_x$′ configuration.

The reason for this symmetry breaking is that in neither component of a pure ^{3}E′ state of $\mathbf{1}^-$ does the distribution of negative charge in the π space have D_{3h} symmetry (i.e., transform as the a$_1$′ representation of D_{3h}). Coulombic repulsion between the σ and π electrons then produces a distribution of charge in the σ space that also has only C_{2v} not D_{3h} symmetry; this in turn mixes ^{3}E$_x$′ with the low-lying ^{3}A$_2$′ state in the π space. In theory, the same mixing can occur between ^{3}E$_y$′ and ^{3}A$_1$′, but this mixing is found to be negligible because ^{3}A$_1$′ is a much higher-lying excited state than ^{3}A$_2$′.[38] The ^{3}A$_2$′ contaminant of ^{3}E$_x$′ accounts for the slightly different energies computed for ^{3}E$_x$′ and ^{3}E$_y$′ at both the CASSCF and CASPT2N levels of theory.[21]

Attempts to perform CASSCF calculations on the ^{3}A$_2$′ state of $\mathbf{1}^-$ initially met with failure. ^{3}A$_2$ is the second ^{3}B$_2$ state in C_{2v} symmetry, and CASSCF calculations on the second ^{3}B$_2$ state failed to converge.[39] CASSCF wave functions for both states were obtained by first optimizing the σ and π CASSCF MOs for an average state, containing both ^{3}B$_2$ states (^{3}E$_x$′ and ^{3}A$_2$′) and then optimizing the CASSCF π wave functions for the individual states. The average σ MOs that resulted were less distorted than when the CASSCF wave function for just ^{3}E$_x$′ was obtained. Consequently, the energy for ^{3}E$_x$′ from the average CASSCF calculation was 1.6 kcal/mol higher than the energy obtained from a CASSCF calculation on ^{3}E$_x$′ by itself.

The second D_{3h} triplet state, ^{3}A$_2$′, has configuration c as its dominant configuration. Configuration c differs from configurations a and b, the dominant configurations in the ^{3}E′ wave functions, by having the β spin electron in the a$_2$″ NBMO rather than in one of the degenerate pair of e″ NBMOs. This difference in orbital occupancy results in a Coulombic interaction in ^{3}E′ between electrons of opposite spin in the e″ NBMOs being replaced in ^{3}A$_2$′ by one between electrons of opposite spin, one in the a$_2$″ NBMO and the other in the e″ NBMO.

(35) For comparison, twisting of one methylene group out of conjugation raises the energy of triplet *m*-benzoquinodimethane (MBQDM) by 14.2 kcal/mol[36a] and of benzyl radical by 11.9 kcal/mol[36b] at the (8,8)CASSCF/6-31G* and (7,7)CASSCF/6-31G** levels of theory, respectively. The parallel spins in the planar geometries of the ^{4}A$_1$″ state of **1** and the ^{3}B$_2$ state of MBQDM act cooperatively to reverse the order of the barrier heights for methylene rotation from that predicted by Hückel theory: **1** (-0.70β) < MBQDM (-0.71β) < benzyl (-0.72β). The same type of effect has previously been noted in comparing barriers to methylene group rotation in the ^{3}A$_2$′ state of trimethylenemethane and in allyl radical [Getty, S. J.; Hrovat, D. A.; Xu, J. D.; Barker, S. A.; Borden, W. T. *J. Chem. Soc., Faraday Trans.* **1994**, *90*, 1689. See also, ref 11].

(36) (a) Hrovat, D. A.; Borden, W. T. Unpublished results. (b) Hrovat, D. A.; Borden, W. T. *J. Phys. Chem.* **1994**, *98*, 10460.

(37) The twisted geometry is computed to lie higher in energy than the planar structure by 2.5 kcal/mol at CASPT2N/6-31G* and 6.6 kcal/mol at UB3LYP/6-31G*. UB3LYP/6-31G* frequency calculations find the twisted geometry to be the transition state for methylene rotation.

(38) The lowest ^{3}A$_1$′ excited state involves an excitation of an electron out of a π bonding orbital into a NBMO or out of a NBMO into an antibonding π orbital.

(39) This may have been due to the distorted σ core for ^{3}E$_x$′ not being at all optimal for ^{3}A$_2$′, which should prefer a σ core with D_{3h} symmetry.

Since, as discussed above, the latter interaction is of higher energy than the former, $^3A_2'$ is calculated to lie above $^3E'$, at both the CASSCF and MR-CI(π-SD, σ-S)+Q levels of theory.

The remaining pair of low-lying states are both $^1E'$. The lower energy of these two $^1E'$ states, 1 $^1E'$, consists principally of the out-of-phase combinations of configurations e and f for 1 $^1E_y'$ and g and h for 1 $^1E_x'$. The 1 $^1E_x'$ state is the singlet complement of $^3A_2'$. The pair of electrons in the e″ NBMOs, which have the same spin in $^3A_2'$, have opposite spins in the 1 $^1E'$ state.

The higher energy $^1E'$ state, 2 $^1E'$, consists principally of configurations i − j and k − l and is the singlet complement of $^3E'$. The electrons in the singly occupied a_2'' and e″ NBMOs, which have the same spin in $^3E'$, have opposite spin in 2 $^1E'$. The fact that the a_2'' and e″ NBMOs are less disjoint than the e_x'' and e_y'' NBMOs is responsible for the finding that 2 $^1E'$ has a higher energy than 1 $^1E'$, in which electrons in e_x'' and e_y'' have opposite spins.

The two $^1E'$ states of $\mathbf{1}^-$ are both well above the three states of lowest energy, $^3E'$, $^1A_1'$, and $^3A_2'$. The latter three states are all within 6 kcal/mol of each other at the CASSCF level.[40] Inclusion of $\sigma-\pi$ correlation further compresses the CASSCF energy differences between the three lowest-lying states, since their energies span only 1−2 kcal/mol at CASPT2N and 3 kcal/mol at the MR-CI(π-SD, σ-S)+Q CI level of theory.

Because CASPT2N uses second-order perturbation theory, it almost certainly overestimates the compression of the energy differences. Unlike CASPT2N, MR-CI(π-SD, σ-S)+Q is variational, and Table 2 shows that MR-CI appears to give energies at D_{3h} geometries that show little dependence on the set of MOs used. Therefore, the MR-CI calculations, which find $^3E'$ to be the lowest D_{3h} energy state but $^3A_2'$ and $^1A_1'$ both to lie less than 3 kcal/mol higher, probably gives the most accurate energy separations.

Calculations on $\mathbf{1}^-$ at C_{2v} Geometries. With the three lowest states of $\mathbf{1}^-$ being so close in energy at D_{3h} geometries, Jahn−Teller effects play an important role in determining the energy separations between the equilibrium geometries of these states (see Figure 7). Only the $^3E'$ state is subject to a first-order Jahn−Teller effect, and the E_x' component of this state can be further stabilized by second-order Jahn−Teller mixing with $^3A_2'$ upon an e_y' molecular distortion. As shown in Figure 3, this distortion preserves C_{2v} symmetry, and in C_{2v} symmetry, $^3E_x'$ and $^3A_2'$ both become $^3B_2$ states.

The second-order Jahn−Teller mixing of $^3E_x'$ with $^3A_2'$ should lead to the lowest energy C_{2v} state being $^3B_2$. Since $^3E_x'$ is stabilized by the first-order Jahn−Teller effect upon a s-l-l e_y' distortion, the three equivalent s-l-l structures with $^3B_2$ wave functions should be the minima on the lowest energy pseudorotational pathway for the ground state of $\mathbf{1}^-$; and three equivalent l-s-s structures with $^3A_1$ wave functions should be the transition states that connect the minima.

Table 2 shows that, at all levels of theory, the energy decrease upon s-l-l distortion of $^3E_x'$ to $^3B_2$ is nearly a factor of 2 larger in magnitude than the energy lowering upon l-s-s distortion of $^3E_y'$ to $^3A_1$. At both the CASSCF and MR-CI(π-SD,σ-S)+Q levels the $^3B_2$ minima on the pseudorotation pathway for the ground state of $\mathbf{1}^-$ are ca 1.5 kcal/mol lower in energy than the $^3A_1$ transition states.

The $^1A_1'$ state too can be stabilized upon e_y' molecular distortions from D_{3h} symmetry by mixing with the $^1E_y'$ components of the $^1E'$ states. At the CASSCF level, the second-order Jahn−Teller energy lowering of the $^1A_1$ state that results from this mixing is about 1 kcal/mol for both l-s-s and s-l-l distortions to C_{2v} symmetry. However, as Table 2 shows, MR-CI(π-SD,σ-S)+Q calculations at the CASSCF-optimized C_{2v} geometries find either a very small second-order Jahn−Teller stabilization[41] or an energy increase. At the MR-CI(π-SD, σ-S)+Q level of theory, the $^3B_2$ minima on the pseudorotation pathway for the ground state are computed to be ca. 6 kcal/mol lower in energy than the $^1A_1$ (s-l-l) and $^3A_2'$ excited states.

Since $\mathbf{1}^-$ is a carbanion, we investigated the effect of including diffuse functions in the basis set.[22b] CASSCF/6-31+G* calculations found $^3B_2$ still to be the ground state. The energy separations between $^3B_2$ and the $^3A_1$ pseudorotation transition states, the D_{3h} $^1A_1'$ state, and the C_{2v} $^1A_1$ geometries to which the latter distorts were all found to increase by ca. 0.5 kcal/mol. Thus, it does not appear that the presence of diffuse functions in the basis set for $\mathbf{1}^-$ causes any decrease in the energies of the low-lying excited states of this carbanion, relative to the ground state.

Calculations on $\mathbf{1}^-$ at Twisted C_{2v} Geometries. Calculations at (10,9)CASSCF/6-31G* level of theory indicate that there are moderately high barriers to methylene rotation in the $^3B_2$ and $^1A_1$ states of $\mathbf{1}^-$. Structures with one methylene group twisted perpendicular to the benzene ring lie higher than the optimized planar geometries by 11.0 kcal/mol for the triplet and 7.1 kcal/mol for the singlet. At CASPT2N, these barriers to methylene rotation increase to 12.8 kcal/mol for the triplet and 12.7 for the singlet.[42]

In both states, the lowest energy electronic configuration is that of a *m*-benzoquinodimethane radical anion[12] plus one electron in the p orbital on the twisted methylene group. The energies, geometries, and orbitals of the twisted triplet and twisted singlet are nearly identical. The singlet and triplet states in which two electrons occupy the a_2 π NBMO and one electron occupies the b_1 π NBMO are lower in energy by 3−4 kcal/mol than the singlet and triplet states in which the NBMO occupations are reversed.[12]

Electronic states of $\mathbf{1}^-$ in which the twisted p orbital is doubly, rather than singly, occupied are much higher in energy, due to the Coulombic repulsion energy associated with confining two electrons of opposite spin to the same region of space. States in which the twisted p orbital is empty are higher still in energy, due to the even higher Coulomb repulsion energy between the 10 π electrons in the dianion of *meta*-benzoquinodimethane.

Predicted Photoelectron Spectrum of $\mathbf{1}^-$. Upon photodetachment of $\mathbf{1}^-$, $^4A_1''$ is the lowest energy state of **1** that can be formed. This state of **1** has a D_{3h} equilibrium geometry; whereas, the equilibrium geometry of $\mathbf{1}^-$ is predicted to be distorted away from D_{3h} symmetry by first- and second-order Jahn−Teller effects. Consequently, the band in the photoelectron spectrum of $\mathbf{1}^-$ that corresponds to formation of the $^4A_1''$ state of **1** should show vibrational progressions whose frequencies are those of the e′ modes of $^4A_1''$ that alter significantly the C−C bond lengths and angles.

An important pair of e′ modes in this regard is probably the pair shown in Figure 3. However, there are a total of 8 e′ modes in **1**; so the vibrational structure in the first band in the photoelectron spectrum of $\mathbf{1}^-$ could be quite complex. UB3LYP/6-31+G* calculations on $^4A_1''$ give unscaled frequencies of 296, 509, 944, 1063, 1229, 1422, 1511, and 1528 cm^{-1} for the e′

(40) If the triplet states of $\mathbf{1}^-$ are conceptualized as each arising from addition of one electron to the $^4A_1''$ state of **1**, then there is only a small energetic preference for adding the electron to one of the e″ NBMOs, rather than to the a_2'' NBMO.

(41) The energy decrease occurs for the C_{2v} distortion that provides first-order Jahn−Teller stabilization of $^1E_y'$ and thus decreases the energy separation between it and $^1A_1'$ with which it mixes.

(42) UB3LYP/6-31+G* calculations place the twisted triplet state 15.4 kcal/mol above the planar geometry.

modes.[43] The 1229 cm^{-1} frequency corresponds to the mode shown in Figure 3.

Vibrational progressions in the totally symmetric a_1' modes might also be seen. However, the average lengths of the C−C bonds in the ground states of $\mathbf{1}^-$ and **1** (Table 3) are calculated to be almost the same.[44] Therefore, a_1' skeletal modes of $^4A_1''$ may not be visible in the band that corresponds to formation of this state of **1**.

We have calculated the adiabatic electron affinity (EA) of **1**, corresponding to the energy of the (0,0) band of the $^4A_1''$ state of **1** in the photoelectron spectrum. The presence of diffuse functions in the basis set is necessary to make $\mathbf{1}^-$ even bound at the CASPT2N level of theory. For example, with the 6-31G* basis set, loss of an electron from $^3B_2$ to form the $^4A_1''$ ground state of **1** is computed to be exothermic by 37.3 kcal/mol at the CASSCF level and by 9.7 kcal/mol at CASPT2N. With the 6-31+G* basis set, $^3B_2$ is still unbound by 26.8 kcal/mol at the CASSCF level but bound by 5.5 kcal/mol at CASPT2N.

Schaefer and co-workers have found that B3LYP/6-31+G* calculations give reasonably accurate electron affinities.[45−47] We carried out full geometry optimizations at the UB3LYP/6-31+G* level for the lowest states of $\mathbf{1}^-$ and **1**.[48] These UB3LYP calculations find the $^3A_2'$ state of $\mathbf{1}^-$ to lie 0.3 kcal/mol below the $^3A_1$ component of the Jahn−Teller-distorted $^3E'$ state. We were unable to obtain an energy for the Jahn−Teller-distorted $^3B_2$ component of $^3E'$, because in C_{2v} symmetry the D_{3h} $^3A_2'$ state is also $^3B_2$. At all C_{2v} starting geometries that we investigated, geometry optimization of $^3B_2$ led back to the D_{3h} geometry of $^3A_2'$.

The UB3LYP energy ordering, which places $^3A_2'$ below both components of the Jahn−Teller-distorted $^3E'$ state is different from the ordering obtained from both the CASSCF and MR-CI calculations. Nevertheless, in qualitative agreement with the CASSCF and MR-CI results, UB3LYP predicts $^1A_1'$ to distort from D_{3h} to C_{2v} symmetry and finds the resulting $^1A_1$ state to lie 6.4 kcal/mol above the lowest triplet state. However, it should be noted that $S^2 = 1.06$ in the UB3LYP description of $^1A_1$; so at the UB3LYP level, this state is halfway between a singlet and triplet.

UB3LYP/6-31+G* predicts the $^3A_2'$ state of $\mathbf{1}^-$ to be bound by 19.6 kcal/mol, including a correction for zero-point energy differences. With EA ≈ 20 kcal/mol, all of the low-lying states of $\mathbf{1}^-$—$^3A_2'$, the $^3A_1$ and $^3B_2$ components of $^3E'$, and $^1A_1$—should be bound.

In order to assess the reliability of our UB3LYP/6-31+G* results on the EA of **1**, we calculated the EA of benzyl radical at this level of theory. Although benzyl radical lacks two of the exocyclic methylene groups present in **1**, benzyl radical and **1** are structurally related; and the EA of benzyl has been measured.[49] After corrections for ZPE differences between benzyl anion and benzyl radical, UB3LYP/6-31+G* gives EA = 19.3 kcal/mol, which is ca. 2 kcal/mol lower than the experimental value of 21.0 ± 0.1 kcal/mol for benzyl. If a 2 kcal/mol correction is applied to the UB3LYP/6-31+G* value for the EA of **1**, a predicted value of 21−22 kcal/mol is obtained. This is in excellent agreement with a preliminary estimate of the adiabatic EA for **1** of 21.9 ± 1.0 kcal/mol, obtained by the kinetic method.[50]

The position of the first band in the photoelectron spectrum of $\mathbf{1}^-$ will show how accurate this predicted value for the EA of **1** really is.[51] In addition, the vibrational structure in the first band should reveal whether the ground state of $\mathbf{1}^-$ is the D_{3h} $^3A_2'$ state, as predicted by UB3LYP/6-31+G*, or the Jahn−Teller-distorted $^3E'$ state, as predicted by both CASSCF and MR-CI methods. The presence or absence of hot bands in the spectrum will indicate whether UB3LYP/6-31+G* is correct in predicting the lowest excited state of $\mathbf{1}^-$ to be <1 kcal/mol above the ground state or whether, as predicted by both CASSCF and MR-CI, the lowest excited state of $\mathbf{1}^-$ is >5 kcal/mol above the ground state. Finally, the splitting between the first band and the second band in the spectrum[52] will show which is more accurate for the energy separation between the $^4A_1''$ ground state of **1** and the Jahn−Teller distorted $^2E''$ state: the UB3LYP figure of 10 kcal/mol[48] or the *ab initio* value of 14 ± 1 kcal/mol.

We look forward to the measurement of the photoelectron spectrum of $\mathbf{1}^-$, so that the accuracy of these computational predictions can be assessed by comparison with experiment.

Acknowledgment. This manuscript is dedicated to the memory of Paul Dowd, a pioneer in the experimental study of diradicals. We thank the National Science Foundation for funding of this research and Dr. David Hrovat for his assistance.

JA970195J

(43) ROHF/3-21G calculations provide unscaled frequencies of 317, 580, 1028, 1132, 1272, 1590, 1625, and 1715 cm^{-1} for these modes. The ROHF values may be subject to significant errors because the ROHF formalism does not account for correlation between electrons of opposite spin.[21]

(44) Even after inclusion of diffuse functions in the basis set the average C−C bond distances in $\mathbf{1}^-$ remain very close to those calculated for **1**.

(45) (a) Schaefer, H. F., III *THEOCHEM* In press. (b) Galbraith, J. M.; Schaefer, H. F., III *J. Chem. Phys.* **1996**, *105*, 862. (c) Tschumper, G. S.; Fermann, J. T.; Schaefer, H. F., III *J. Chem. Phys.* **1996**, *104*, 3676. (d) King, R. A.; Galbraith, J. M.; Schaefer, H. F., III *J. Phys. Chem.* **1996**, *100*, 6061.

(46) Using B3LYP/6-31+G*, the EA of cyclooctatetraene is overestimated by 0.24 eV,[47a] compared to the experimental value.[13] In contrast, the EA is underestimated by 0.52 eV at the CASPT2N/6-31+G*//(8,8)-CASSCF/6-31G* level.[47b]

(47) (a) Hrovat, D. A.; Hammons, J. A.; Stevenson, C. D.; Borden, W. T. *S*ubmitted. (b) Hrovat, D. A.; Bartlett, K. L.; Borden, W. T. Unpublished results.

(48) Using UB3LYP/6-31+G*, the $^2A_2$ state lies 10.7 kcal/mol higher than $^4A_1''$. The UB3LYP zero-point energy correction is similar to that found at the (3,3)CASSCF/3-21G level of theory and decreases the doublet−quartet splitting to 10.1 kcal/mol. This UB3LYP value is only about 70% as large as the energy differences predicted by our CASSCF, CASPT2N, and MR-CI calculations. The origin of this discrepancy is probably that the UB3LYP calculations on $^2A_2$, like the UHF calculations on this state,[10] have serious spin contamination problems ($S^2 = 1.78$). The spin contamination arises because, as discussed in the text, a minimal description of $^2A_2$ requires at least two configurations [c and d in Figure 2].

(49) Gunion, R.; Gilles, M. K.; Polak, M.; Lineberger, W. C. *Int. J. Mass Spectrom. Ion Processes* **1992**, *117*, 601.

(50) Hu, J.; Squires, R. R. Unpublished results.

(51) If $^1A_1'$ were the ground state of $\mathbf{1}^-$, a very different apparent EA might be inferred from the photoelectron spectrum, because formation of a quartet by loss of one electron from a singlet is a spin-forbidden transition. Therefore, the $^1A_1'$ to $^4A_1''$ band might be very weak or absent in the photoelectron spectrum of $\mathbf{1}^-$.

(52) The vibrational structure in the band corresponding to loss of an electron from the Jahn−Teller distorted $^3E'$ state of $\mathbf{1}^-$ to form the Jahn−Teller distorted $^2E''$ state of **1** could be very complex.